Available online at www.sciencedirect.com

ScienceDirect

Physics Procedia 83 (2016) 1253 – 1260

Physics Procedia

9th International Conference on Photonic Technologies - LANE 2016

High resolution temperature estimation during laser cladding of stainless steel

Wim Devesse[a,*], Dieter De Baere[a], Michaël Hinderdael[a], Patrick Guillaume[a]

[a]*Vrije Universiteit Brussel, Acoustics and Vibration Research Group, Pleinlaan 2, B-1050 Brussels, Belgium*

Abstract

Laser cladding is a technique that is used for the coating, repair and production of metallic parts. Material is added to the surface of the part by injecting a flow of powder into a melt pool that is created with a high power laser beam. When the beam scans the surface of the substrate, strong local heating and cooling results. A good knowledge of the temperature distribution history during the laser cladding process is vital to predict and optimize the material properties of the final part. This paper presents a contactless temperature measurement system with high temporal and spatial resolution based on a hyperspectral line camera. High temperature measurements were made during laser cladding of AISI 316L stainless steel. A good correlation is shown between the temperature measurements and microscope images taken after creation of the clad.

Peer-review under responsibility of the Bayerisches Laserzentrum GmbH

Keywords: Laser cladding; additive manufacturing; temperature measurement; hyperspectral imaging

1. Introduction

Laser cladding is a technology that is frequently used for applying coatings on metallic parts. It is also a cost-effective technique for repairing parts that show excessive wear. An emerging trend is the use of laser cladding as an additive manufacturing technique for producing freeform metallic parts, in which case it is also known as laser metal deposition (Toyserkani et al., 2005). During this process a high power laser beam is focused on the surface of a solid metallic workpiece, where it locally heats the material until a melt pool is created. Metallic powder is blown into the melt pool and mixes with the molten substrate material. The nozzle is then moved such that the melt pool solidifies

* Corresponding author. Tel.: +32-485-545-913 .
E-mail address: Wim.Devesse@vub.ac.be

Peer-review under responsibility of the Bayerisches Laserzentrum GmbH
doi:10.1016/j.phpro.2016.08.132

and a track of solid material (a clad) is formed. Moving the nozzle according to a predetermined path allows the creation of the desired near net shape product.

The quality of the cladded layers is strongly dictated by the temperature history of the substrate during the manufacturing process. A lot of research is therefore directed towards the design of effective melt pool monitoring methods which can acquire reliable temperature information, possibly to be used in automatic feedback control systems (Salehi and Brandt, 2006; Bi et al., 2006; Song and Mazumder, 2011). As a pool of liquid metal presents a destructive environment for typical contact temperature sensors, and the melt pool properties themselves would also be disturbed by such a sensor, a contactless measurement system is preferred. In the past, multiwavelength pyrometers with one, two or more colors have been used to provide point measurements of the temperature in the melt pool during laser welding and laser cladding processes (Doubenskaia et al., 2006, 2013; Muller et al., 2012). These methods have the inherent drawback that the variation of emissivity with wavelength needs to be known in order to calculate a temperature value from the measured radiance values (Coates, 1981; Khan et al., 1991; Gathers, 1992). Because this information is usually not available, an assumption such as treating the object as a gray body needs to be used, which is not always appropriate. The use of a pyrometer as a temperature measurement device presents some additional drawbacks such as the difficulty of focusing on a very small spot with a known location and a high sensitivity to noise.

In this paper, the use of a hyperspectral line camera is presented as a means to obtain the spectra of a large number of closely spaced points at many different wavelengths. The temperatures of the points can be deduced from the spectra using a suitable curve fitting mechanism, thereby significantly increasing the signal-to-noise ratio compared to methods that use only a small number of wavelengths. However, the biggest advantage of this system is that it results in a temperature profile of the melt pool surface with a very high spatial resolution. Such temperature profiles present useful information about the change of temperature inside the melt pool, which is not practical to obtain with the use of pyrometers alone.

The paper starts by presenting the equations needed for determining the absolute temperature from a measurement of the spectrum. The experimental setup is then presented in Section 3 and followed by the presentation and discussion of a number of measurements made during laser melting and laser cladding of stainless steel in Section 4. Final remarks and conclusions are formulated in Section 5.

2. Temperature estimation

Planck's law (Planck, 1913) states that the spectral radiance emitted by an ideal black body can be written as a function of the wavelength λ and the temperature T:

$$B(\lambda,T)=\frac{2hc^2}{\lambda^5}\frac{1}{\exp\left(\frac{hc}{k_B\lambda T}\right)-1} \tag{1}$$

In this equation, c is the speed of light, h is the Planck constant and k_B is the Boltzmann constant. An ideal black body does not exist in reality, but the spectral radiance of a real body can be described by the black body radiation multiplied with a spectral emissivity ε_λ, which must have a value between 0 and 1. In addition, a measurement of the spectral radiation E_i at a wavelength λ_i ($i = 1,\ldots,N$) will include some measurement noise n_i:

$$E_i=\varepsilon_\lambda(\lambda_i)\cdot B(\lambda_i,T)+n_i \tag{2}$$

The emissivity is written down as an explicit function of λ_i, to emphasize that it is a wavelength dependent quantity. A frequently made assumption is that the emissivity is wavelength independent in the spectral region of interest. This leads to the so-called gray body description in which ε_λ is equal to a constant value:

$$\varepsilon_\lambda(\lambda_i)=\varepsilon \tag{3}$$

Assuming that the noise n_i is zero-mean and Gaussian distributed with variance σ_i^2, the maximum likelihood estimates of the temperature T and emissivity ε given the measurements E_i are obtained by solving a nonlinear least squares problem:

$$\left(\varepsilon_u, T_u\right) = \arg\min_{(\varepsilon,T)} \sum_{i=1}^{N} \frac{\left|E_i - \varepsilon \cdot B\left(\lambda_i, T\right)\right|^2}{\sigma_i^2} \tag{4}$$

The cost function in Eq. (4) includes a weighting which is inversely proportional to the variance of the measurements σ_i^2. This ensures that samples which have a large uncertainty (large variance) have a small influence on the calculated estimates.

For metals it can be shown theoretically that the emissivity must be a decreasing function of wavelength for large wavelengths (Hagen and Rubens, 1903). This has been confirmed in numerous experiments and shown to hold for stainless steels for smaller wavelengths up to the near infrared and visible region (Coblentz and Stair, 1929; Yoshiharu and Hideo, 1980; Yoshiharu, 1983; Zwinkels et al., 1994). Knowing that the emissivity can never be larger than 1, an upper bound for ε_λ can be written as a decreasing function of wavelength with average value ε:

$$\varepsilon_\lambda\left(\lambda_i\right) = 1 - 2\left(1-\varepsilon\right)\frac{\lambda_i - \lambda_1}{\lambda_N - \lambda_1} \tag{5}$$

The least squares problem then becomes:

$$\left(\varepsilon_l, T_l\right) = \arg\min_{(\varepsilon,T)} \sum_{i=1}^{N} \frac{\left|E_i - \left(1 - 2\left(1-\varepsilon\right)\frac{\lambda_i - \lambda_1}{\lambda_N - \lambda_1}\right) \cdot B\left(\lambda_i, T\right)\right|^2}{\sigma_i^2} \tag{6}$$

If the noise is indeed zero-mean, Gaussian distributed and no systematic errors are present in the measurements, the true temperature value must lie between the expected values of the lower bound T_l and upper bound T_u.

3. Experimental setup

The measurements were performed with a SPECIM PFD V10E hyperspectral line camera. The camera is sensitive in the visible and near infrared (VNIR) region from 400 nm to 950 nm. It can measure the spectra of a large number of adjacent points on a line with a spectral resolution of 1.1 nm/pixel and a spatial resolution of 12 µm/pixel. The spectrum of each spatial point can be used to estimate the corresponding temperature using the least squares minimization approach described in Section 2. The images containing the spectra were captured with an exposure time of 78 µs at a frame rate of 1000 frames per second and transferred to a frame grabber over a CameraLink interface for storage and analysis on a personal computer. The MATLAB software was used to perform the nonlinear least squares calculations.

An absolute calibration of the camera was performed by measuring the spectrum of an Optronic Laboratories OL455 integrating sphere calibration source with a halogen lamp. The same spectrum was measured with a NIST traceable JETI Specbos 1211 spectroradiometer. The ratio of these two spectra can then be used to correct the measurements made during the actual experiments before running the temperature estimation algorithm.

During the experiments, the camera was focused on a substrate of AISI 316L stainless steel at an angle of 38 degrees relative to the surface normal. The substrate was moving at a constant speed of 0.5 m/min. A 1 kW fiber laser (IPG YLS-1000) having a flat top laser beam with 1.2 mm diameter was focused on the same location and used to create a melt pool by heating the substrate. Different melt pool sizes can be created by using different laser power values. Figure 1 gives an overview of the measurement setup and the location of the camera focus. The camera was used to measure the spectra of the points on a line at the center of the melt pool, perpendicular to the direction of

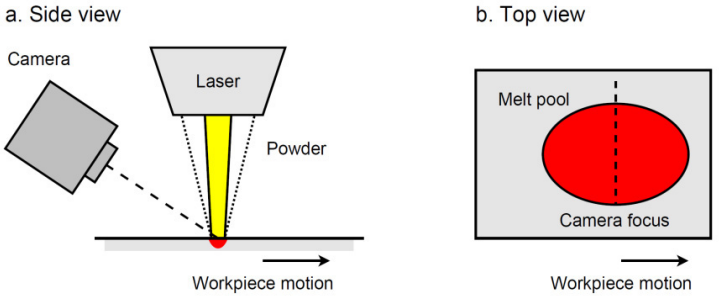

Fig. 1. Side view (left) and top view (right) of the measurement setup.

movement of the workpiece, indicated as the dashed line in Figure 1b. In this way, a cross-section of the surface melt pool temperature distribution can be obtained. The experiments were performed in an Argon gas environment to minimize oxidation of the melt pool surface. In addition to this laser melting process, a laser cladding operation can be performed by switching on a coaxial flow of metal powder particles with a mass flow rate of 2.1 g/min. The used powder is LPW 316L 44-106 µm and it is fed to the nozzle (Fraunhofer ILT COAX-40-S) using a Medicoat CH-5506 powder feeder.

4. Results and discussion

In this section, the temperature and emissivity measurements for a number of experiments are presented. First, the accuracy of the measurement setup is illustrated with a laser melting process. This is a steady process with very small fluctuations and can be used to validate the results. Adding a powder flow to the process results in noisier measurements which still contain valuable information of the melt pool surface temperature.

4.1. Laser melting

Figure 2a shows the steady state temperature profile of a cross-section of the melt pool surface during a laser melting experiment with a laser power of 350 W, resulting in an irradiance of 310 W/mm^2. The measurements are time averages of 100 measurements at a frame rate of 1000 frames per second, i.e. one measurement per ms. The upper curve is the upper bound, in which a gray body assumption is made and the temperatures are estimated using Eq. (4). The lower bound corresponds to the estimates with a decreasing emissivity value starting from 1, using Eq. (6). Figure 2b shows the corresponding estimated emissivity profiles.

The data shown in Fig. 2 is valid only between x = -0.6 mm and x = 0.6 mm because of the effects of stray light. Due to imperfections in the camera optics, some of the light is refracted to a wrong location on the camera sensor. This means that the spectrum which is present near the center of the melt pool (x = 0) can also be measured near the image boundaries ($|x|$ > 0.6 mm). Even though the signal level of this stray light is small (smaller than 0.5% of the original signal level) it is still larger than that of the actual spectrum at those locations. The temperature estimation will therefore try to fit the spectrum of the stray light and obtain an incorrect temperature value. This explains the apparent rise in temperature near the edges of the image, which is not physically possible.

The maximum melt pool temperature is situated between 2000 K and 2200 K, which translates to an uncertainty of roughly 10%. The temperature decreases monotonously towards the boundary of the melt pool but a relative difference of 10% between the upper and lower temperature bounds is maintained. It is clearly visible where the melt pool boundary is situated: around $|x|$ = 0.5 mm the slope of the upper temperature bound decreases. This is an indication that the material is undergoing a phase change and that the melt pool boundary should be situated here. This can be confirmed by looking at the absolute temperature values: the lower and upper temperature bounds at $|x|$ = 0.5 mm are 1590 K and 1760 K respectively. This interval includes the melting point of AISI 316L stainless steel, which is approximately 1670 K (Davis, 1998). The melting point is indicated on the plots as a horizontal dotted line.

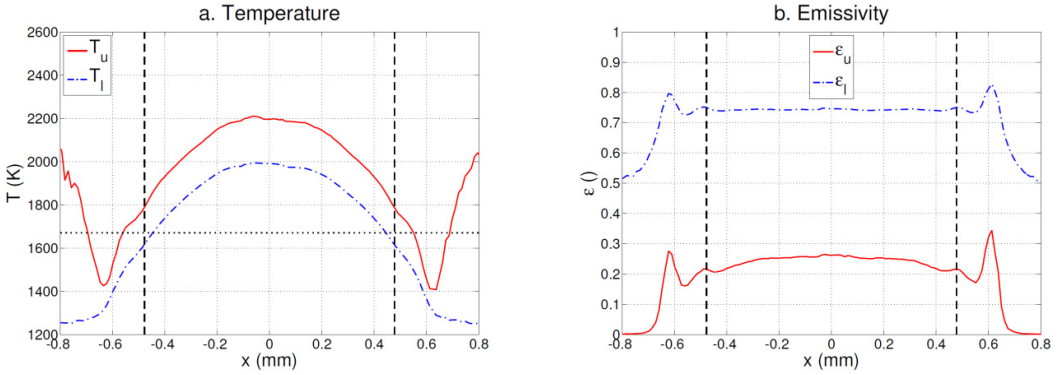

Fig. 2. Temperature (left) and emissivity (right) profiles for a low power laser melting experiment. Solid curves correspond to the upper temperature bound and dash-dotted curves to the lower temperature bound. Dashed vertical lines indicate the melt pool boundary.

Looking at Fig. 2b it can be seen that the emissivity remains relatively constant over the complete melt pool surface. A small increase with temperature can be noted, which may be due to a small temperature dependence of the emissivity and/or a curvature of the melt pool surface. It must be remembered that the reported emissivity values are not normal emissivities because the camera looks at the melt pool with a nonzero angle of approximately 38 degrees. Since the position of the camera with respect to the melt pool is fixed, a local change of the melt pool surface normal results in a change in the measured emissivity. Near the boundary of the melt pool, a small increase of the emissivity can be noticed, which is due to the phase change of the material. The appearance of the larger peaks around $|x| = 0.65$ mm is possibly a result of the stray light interfering with the actual spectrum. However, the fact that the peaks are situated close the boundary of the laser beam (0.6 mm) suggests an alternative explanation: due to the interaction of the laser beam with the substrate material, the absorptivity of the substrate (and hence its emissivity) is decreased. The region that was not irradiated by the beam will then have a higher emissivity, which could explain the sudden emissivity increase. For $|x| > 0.65$ mm the emissivity decreases further down to near zero, which is due to the fact that the stray light is predominant here and has a very small signal level.

Figure 3a shows a microscope image of the substrate surface taken after creating the track. From this image the width of the melt pool during the laser melting process can be derived and was found to be 956 ± 21 µm. The corresponding melt pool boundary is marked on the temperature and emissivity plots of Fig. 2 as the dashed vertical lines. This value of 956 µm is in very good correspondence with the observed melt pool boundary locations from the curves as described in the previous paragraphs.

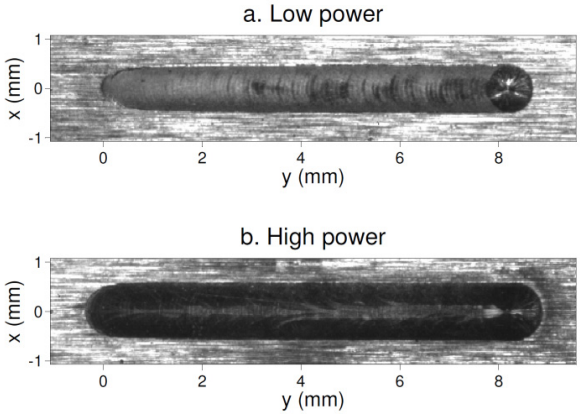

Fig. 3. Microscope images of the tracks created during the low power (top) and high power (bottom) laser melting experiments.

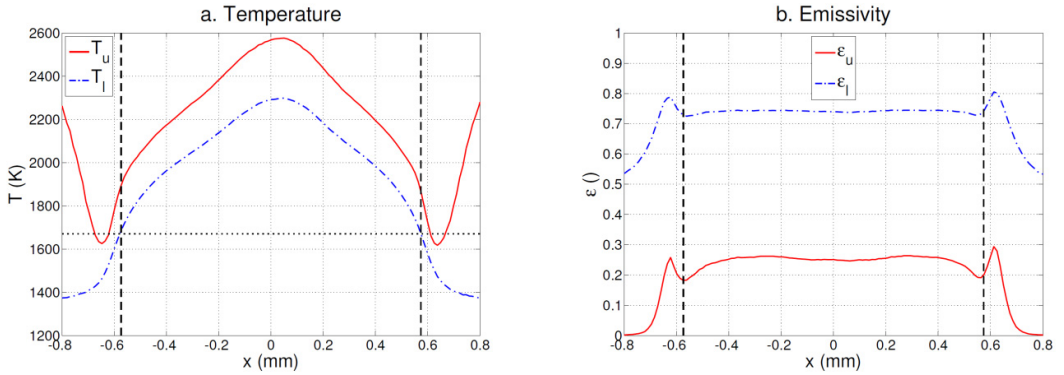

Fig. 4. Temperature (left) and emissivity (right) profiles for a high power laser melting experiment. Solid curves correspond to the upper temperature bound and dash-dotted curves to the lower temperature bound. Dashed vertical lines indicate the melt pool boundary.

Figure 4 contains the measured temperature and emissivity profiles for a similar laser melting experiment with a significantly higher laser power of 500 W (irradiance of 440 W/mm^2). The peak temperature is 400 K higher than in the low power experiment and the temperature shows a linear trend in the liquid region. The melt pool boundary is not as clearly visible as in the low power case, but it can still be observed as a sudden change in the slope of the temperature profile. The emissivity curves show a similar behavior as in the low power experiment, but the local emissivity peaks due to a phase change cannot be discerned from the larger peaks. A microscope image of this track is presented in Fig. 3b and gives a track width of 1147 ± 21 µm. This is again in very good correspondence with the temperature and emissivity measurements.

4.2. Laser cladding

The laser melting experiments presented in Section 4.1 show that the hyperspectral imaging system is capable of determining the absolute temperature profile of the melt pool during the process, which can be directly compared to microscope measurements of the track. By switching on a flow of powder particles, a clad of material can be created on top of the substrate. It is not straightforward to directly compare microscope images of the workpiece to the temperature measurements made during the cladding process because the deposited clads typically bulge out a bit and are therefore wider than the melt pool itself. However, thanks to the confidence in the measurement setup gained from the laser melting results we can still make some interesting conclusions from such measurements.

Figures 5 and 6 show the measured temperature and emissivity profiles of two laser cladding experiments with a laser power of 350 W and 500 W respectively (irradiance of 310 W/mm^2 and 440 W/mm^2). An important difference with the laser melting experiments is that the temperatures are much lower and more evenly distributed inside the melt pool. This can be attributed to the large amount of powder particles that enter the melt pool. Each time a particle enters the melt pool, the liquid spreads out, resulting in a better mixing of the fluid and a more homogeneous temperature distribution.

The emissivity peaks around $|x| = 0.65$ mm are located at the same positions as in the laser melting experiments but they have much larger peak values. The melt pool width can still be clearly resolved from the measurements in Figs. 5 and 6 due to the presence of the small emissivity peaks and change in temperature slope around $|x| = 0.5$ mm and $|x| = 0.57$ mm for the low power and high power experiment respectively. The melt pool widths can therefore be estimated as approximately 1000 µm and 1140 µm. The clad widths can be extracted from the microscope pictures given in Fig. 7 and are determined to be 1190 ± 21 µm and 1232 ± 21 µm. As expected, these clad widths are a bit larger than the estimated melt pool widths. Note that the clad created during the high power experiment is not much wider than that of the low power experiment.

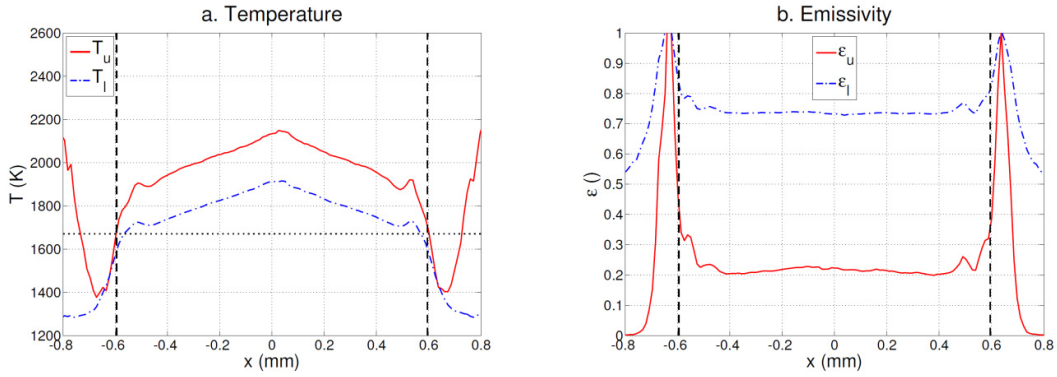

Fig. 5. Temperature (left) and emissivity (right) profiles for a low power laser cladding experiment. Solid curves correspond to the upper temperature bound and dash-dotted curves to the lower temperature bound. Dashed vertical lines indicate the clad boundary.

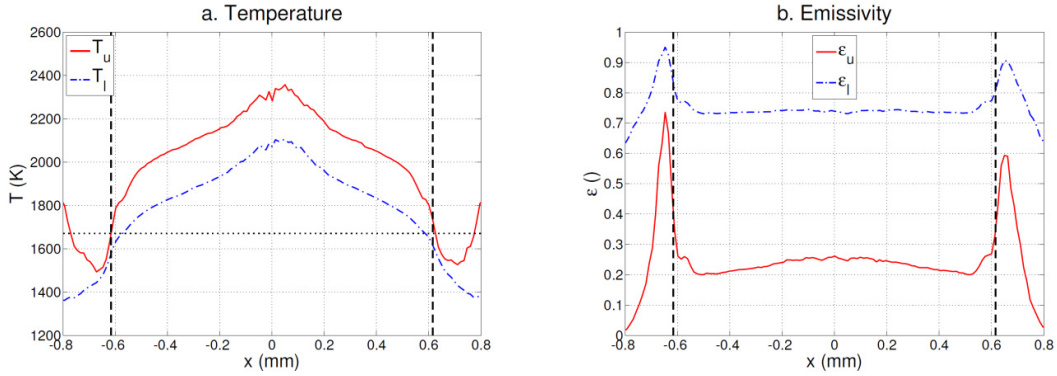

Fig. 6. Temperature (left) and emissivity (right) profiles for a high power laser cladding experiment. Solid curves correspond to the upper temperature bound and dash-dotted curves to the lower temperature bound. Dashed vertical lines indicate the clad boundary.

5. Conclusions

In this paper a method is presented for measuring the surface temperature distribution of a melt pool during laser melting and laser cladding with a hyperspectral line camera. The system is able to measure absolute temperature values in the liquid region of a melt pool of AISI 316L stainless steel with an uncertainty of ca. 10%. The melt pool boundary can be clearly detected and corresponds well to the boundary obtained from microscope images of the tracks. Reliable temperature measurements of the solid region are harder to obtain due to the use of a camera system that is sensitive in the visible and near infrared region. If low temperature information is required, a hyperspectral camera that is sensitive in the short wavelength infrared region should be considered.

Melt pool temperature measurements such as the ones presented in this paper contain valuable information for validating the results of numerical simulations of the laser melting and cladding processes. In addition, the effect of using different laser powers and beam profiles on the hydrodynamic behavior of the melt pool during the process can be quantitatively investigated. This information is useful for performing an optimization of the used laser beam parameters in order to obtain high quality clads.

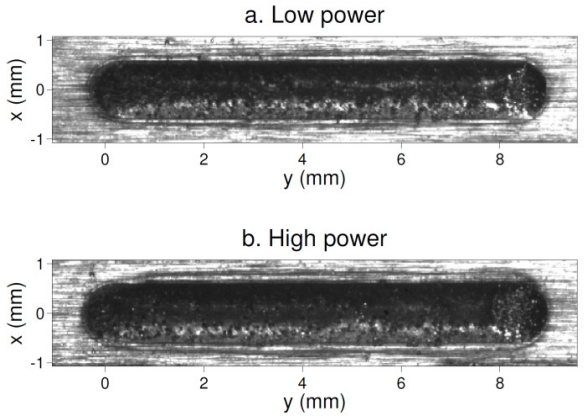

Fig. 7. Microscope images of the clads created during the low power (top) and high power (bottom) laser cladding experiments.

Acknowledgements

This work was supported by the Agency for Innovation by Science and Technology in Flanders (IWT) within the SBO 110070 eSHM with AM project, and the Research Foundation - Flanders (FWO).

References

Bi, G., Gasser, A., Wissenbach, K., Drenker, A., Poprawe, R., 2006. Identification and Qualification of Temperature Signal for Monitoring and Control in Laser Cladding. Optics and Lasers in Engineering 44, 1348-1359.

Coates, P.B., 1981. Multi-Wavelength Pyrometry. Metrologia 17, 103-109.

Coblentz, W.W., Stair, R., 1929. Reflecting Power of Beryllium, Chromium and Several Other Metals. Bureau of Standards Journal of Research 2, 343-354.

Davis, J.R., 1998. Metals Handbook Desk Edition, 2nd ed. ASM International, Ohio.

Doubenskaia, M., Bertrand, Ph., Smurov, I., 2006. Pyrometry in Laser Surface Treatment. Surface & Coatings Technology 201, 1955-1961.

Doubenskaia, M., Pavlov, M., Grigoriev, S., Smurov, I., 2013. Definition of Brightness Temperature and Restoration of True Temperature in Laser Cladding Using Infrared Camera. Surface & Coatings Technology 220, 244-247.

Gathers, G.R., 1992. Analysis of Multiwavelength Pyrometry Using Nonlinear Chi-Square Fits and Monte Carlo Methods. International Journal of Thermophysics 13, 539-554.

Hagen, E., Rubens, H., 1903. Über Beziehungen des Reflexions- und Emissionsvermögens der Metalle zu Ihrem Elektrischen Leitvermögen. Annalen der Physik 316, 873-901.

Khan, M.A., Allemand, C., Eagar, T.W., 1991. Noncontact Temperature Measurement. I. Interpolation Based Techniques. Review of Scientific Instruments 62, 392-402.

Muller, M., Fabbro, R., El-Rabii, H., Hirano, K., 2012. Temperature Measurement of Laser Heated Metals in Highly Oxidizing Environment Using 2D Single-Band and Spectral Pyrometry. Journal of Laser Applications 24, 022006.

Planck, M., 1913. Vorlesungen Über die Theorie der Wärmestrahlung. J.A. Barth, Leipzig.

Salehi, D., Brandt, M., 2006. Melt Pool Temperature Control Using LabVIEW in Nd:YAG Laser Blown Powder Cladding Process. International Journal of Advanced Manufacturing Technology 29, 273-278.

Song, L., Mazumder, J., 2011. Feedback Control of Melt Pool Temperature During Laser Cladding Process. IEEE Transactions on Control Systems Technology 19, 1349-1356.

Toyserkani, E., Khajepour, A., Corbin, S., 2005. Laser Cladding. CRC Press, Boca Raton.

Yoshiharu, N., Hideo, T., 1980. Surface Properties of Polished Stainless Steel. Annals of the CIRP 29, 409-412.

Yoshiharu, N., 1983. Specular Spectral Reflectance of AISI304 Stainless Steel at Near-Normal Incidence. SPIE Proceedings 362, 93-103.

Zwinkels, J.C., Noël, M., Dodd, C.X., 1994. Procedures and Standards for Accurate Spectrophotometric Measurements of Specular Reflectance. Applied Optics 33, 7933-7944.